Application of Orientation Sensing to Robust Long Term SLAM

Saurav Agarwal Suman Chakravorty

***Abstract*—A difficult aspect of SLAM is the problem of uncertainty constrained point-to-point navigation where global loop closures to eliminate estimation biases may not be possible. In such scenarios, a prime concern is to control the rate of localization error growth. We study the SLAM problem when a noisy unbiased heading sensor is available to a robot. We develop fundamental results on the underlying problem of localization and the behavior of loop-closure when heading is available.**

***Index Terms*—Mobile Robots, Autonomous Systems, Simultaneous Localization and Mapping, Navigation**

I. Introduction

When a robot is not given a priori knowledge of its environment, it must use its sensory data and actions to concurrently build a map of its environment and localize itself within its stochastic map, this is referred to as Simultaneous Localization and Mapping (SLAM) [1]. In SLAM, estimation errors tend to build up during exploratory motion and are usually negated by revisiting previously seen locations (loop closure). An important example of application of such robots is planetary rovers. These robots do not have access to global positioning signals and during the course of their missions traverse long trajectories (long-term point-to-point navigation) from their landing site to far-off locations for scientific missions. Thus to conduct missions, rovers often rely on odometry from on-board systems for positioning which may be unreliable. Certain mobile robotics applications, e.g., autonomous military vehicles may require robots to accurately traverse long trajectories wherein global localization information (e.g., GPS) may be degraded due to jamming or spoofing.

A key reason for estimation drift during exploration is the robot heading uncertainty. In common practice, it is assumed that reliable absolute orientation measurements are *not* available in SLAM. Thus existing methods rely on odometery and relative pose or feature measurements to estimate robot orientation and position. In this work we explore the role of absolute orientation sensing in SLAM and its impact on point-to-point autonomous navigation. We ask the question, "Is there a way for a robot to sense its orientation robustly without relying on odometery or local relative measurements?", the answer as it turns out is *yes*. State-of-the-art Visual-Inertial localization methods [2, 3] exhibit error of $\approx 0.3\% - 0.5\%$ which may be unsuitable for precision tasks, e.g. for a 25 km trajectory, it results in 75 m $-$ 125 m position error. In Section V we show that it is possible to attain an accuracy of 0.0006% for a 107.9 km trajectory without loops using existing absolute orientation sensor technology. In fact, such sensors are being mandated for GPS-denied navigation on military aircraft and ships [4, 5].

In the following section we discuss relevant related work. In Section III we state the problem definition and subsequently, in Section IV we present our approach. In Section V we present simulation results for a robot that visits a pre-determined sequence of waypoints followed by conclusions in Section VI.

II. Related Work

There exist two mainstream approaches for solving the SLAM problem; filtering-based methods which maintain a recursive estimate over current robot pose and map; and graph-based methods where robot poses are treated as nodes of a graph and constraints as edges, these solve the full-SLAM problem. In filtering-based SLAM [6], the work of [7] derives analytical upper bounds on state estimate covariance as functions of robot sensor and map characteristics without absolute orientation measurements. The analysis of [8] shows that heading is unobservable in the EKF-SLAM formulation. Several works [8–11] analyze the consistency of EFK-SLAM and show that heading estimation errors are the leading cause of inconsistency due to erroneous Jacobian computations. In [12] the authors show that even for the simple case of a stationary robot with zero process noise observing 1 feature, its heading estimate drifts. The general consensus from aforementioned works being that EKF-SLAM filter tends to become overconfident, i.e., uncertainty estimates do not reflect the true error and heading uncertainty is a major cause of inconsistency.

In graph-based SLAM [13–17], non-linear optimization techniques are used to solve for the maximum likelihood estimate. A major drawback of graph-based SLAM techniques is the reliance on an initial guess to bootstrap the optimizer. This initial guess usually comes from odometery and can be arbitrarily bad leading to local minima. A special property of SLAM is that when robot orientation is known, SLAM can be posed as a linear estimation problem in position. Recent works [18–21] have exploited this structural property with the aim of decoupling non-linearities that arise due to orientation. The works of [18, 19] demonstrate that estimating orientation as

 Saurav Agarwal (sauravag@tamu.edu) and Suman Chakravorty (schakrav@tamu.edu) are with the Department of Aerospace Engineering, Texas A&M University, College Station, TX 77843, USA.

the first step and using these estimates to initialize pose graph optimization results in a robust solution. However guarantees on global optimality of the orientation solution for pose-graph SLAM remained a tricky problem. In [22], the authors made a significant step forward on this problem, showing that the theory of Lagrangian duality allows to compute a globally optimal solution for the SLAM problem in 2D under conditions that are satisfied under noise regimes of practical interest. Further, in [23] the authors develop a method to solve for globally optimal solutions for the robot pose given certain restrictions on noise characteristics of relative pose measurements. The key contribution being a semi-definite relaxation of the Maximum Likelihood Estimator (MLE) whose minimizer provides an exact MLE. We now proceed to discuss absolute orientation sensing and its potential to make SLAM robust, accurate and reliable for long-term autonomy.

A. Absolute Orientation Sensing

Modern star trackers are automated camera-based devices that compute inertial attitude with high accuracy by using measurements to known celestial bodies and comparing them to star charts (e.g., low-cost systems [24] can easily deliver RMS error down to 10 arcseconds or $0.0028°$). Star trackers are extremely robust as they rely on measurements to persistent beacons in space whose trajectories across the sky relative to Earth or other planets can be fixed with great precision from long-term astronomical observations. Star trackers are used heavily in satellite and space probe navigation [25] as well as on ships and aircraft as a backup navigational source when GPS is unavailable [4, 5] during both day and night operation. The method of using stars to navigate is called celestial navigation.

In the domain of mobile robotics, celestial navigation has been proposed for planetary rovers as an alternative to existing methods. Current onboard navigation techniques for planetary rovers include fusing inertial measurement units (IMU) with wheel odometery or using visual odometery [26]. In ground-based tests, visual odometery based localization for the Mars Exploration Rover (MER) [26] achieves an accuracy of 2.5% absolute position error over a 24 m course of driving; this may limit how far a rover can traverse accurately during its mission life while relying purely on onboard sensors. In [27] a lunar positioning method is developed that utilizes star tracking and inclinometers however the positioning error is highly sensitive to inclinometer error. Another sensor that aids absolute heading estimation is a sun sensor and has also been proposed for planetary rovers [28, 29]. We note that sun-sensors (error $\approx 1°$ [29]) are not as accurate as star-trackers and do not allow full 3 degree of freedom (DoF) rotation estimation. In [30] an absolute heading estimation technique based on sun-sensing, inclinometer measurements and precision timing is developed for planetary rovers with heading estimation errors of the order of few degrees. Compared to [27–31] our method proposes to fuse proprioceptive sensing and exteroceptive sensors such as camera, lidars etc. with star tracking or sun sensors for accurate global navigation. Empirical results show that extremely low localization error (0.0006% of distance traveled) can be easily achieved with star trackers.

While there exist other sensors such as magnetometers and gyrocompasses which can provide absolute heading and may be used within our proposed framework, there may be certain associated drawbacks. Magnetometers only work well when the Earth's magnetic field is not corrupted by external influences. Gyrocompasses measure the planet's rotation to determine accurate heading with respect to (w.r.t) geographic north but are bulky and costly, although Microelectromechanical Systems (MEMS)-based gyrocompasses have been proposed [32], they are not yet ready for practical use. Thus celestial navigation presents the current best solution to the orientation sensing problem. Further, daylight star trackers already exist for the military [33] and can be expected to be available in the commercial domain in coming years.

III. Problem Formulation

A portion of preliminaries presented in this section overlap with previous work in [21] but are provided here for the sake of completeness and clarity. Let x_k, u_k, and z_k represent the system state, control input, and observation at time step k respectively. The state vector $\mathbf{x}_k = [\mathbf{p}_k^T, \boldsymbol{\theta}_k^T]^T$, where $\mathbf{p}_k$ and $\boldsymbol{\theta}_k$ are the robot position and orientation parameter vector respectively. We designate a keyframe pose as ${}^{\kappa}x$. The state evolution model f is denoted as $x_{k+1} = f(x_k, u_k) + w_k$ where $w_k \sim \mathcal{N}(0, \mathbf{Q}_k)$ is zero-mean Gaussian process noise. The measurement model h is denoted as $z_k = h(x_k) + v_k$, where $v_k \sim \mathcal{N}(0, \mathbf{R}_k)$ is zero-mean Gaussian measurement noise. The map (unknown at t_0) is a set of landmarks (features) distributed throughout the environment. We define the j-th landmark as l_j. The observation for landmark l_j at time t_k is denoted by $z_k^j \in z_k$. The non-linear inverse measurement model is denoted by g such that for a given measurement z_k^j and the state x_k at which it was made, g computes the landmark location $l_j = g(x_k, z_k^j)$.

We define ${}^l\mathbf{d}_k^{ij}$ to be the relative feature measurement, i.e., displacement from feature l_i to l_j in robot's local frame at time t_k. The local relative feature measurement ${}^l\mathbf{d}_k^{ij} = {}^l\boldsymbol{\Delta}_k^j - {}^l\boldsymbol{\Delta}_k^i$, where ${}^l\boldsymbol{\Delta}_k^i, {}^l\boldsymbol{\Delta}_k^j$ are relative positions of features l_i and l_j respectively with respect to the robot in its local frame. Let $\mathbf{C}(\boldsymbol{\theta}_k)$ denote the Direction Cosine Matrix (DCM) of the robot orientation at state x_k where $\mathbf{C}$ is a function of orientation parameter $\boldsymbol{\theta}_k$ (e.g., Euler angles, Quaternions etc.). A measurement ${}^l\boldsymbol{\Delta}_k^i$ in the robot's local frame can be projected into the world (global) frame as

$$\mathbf{l}_i - \mathbf{p}_k = \underbrace{{}^w\boldsymbol{\Delta}_k^i}_{\text{world frame measurement}} = \mathbf{C}(\boldsymbol{\theta}_k)^T \, {}^l\boldsymbol{\Delta}_k^i, \qquad (1)$$

where $\mathbf{l}_i$ and $\mathbf{p}_k$ are the feature and robot positions in the world frame, see Fig. 1(a).

Currently, the focus of this work is on analyzing the effect of orientation, thus we do not model obstacles in simulation studies. Additionally in Section V we limit the simulation

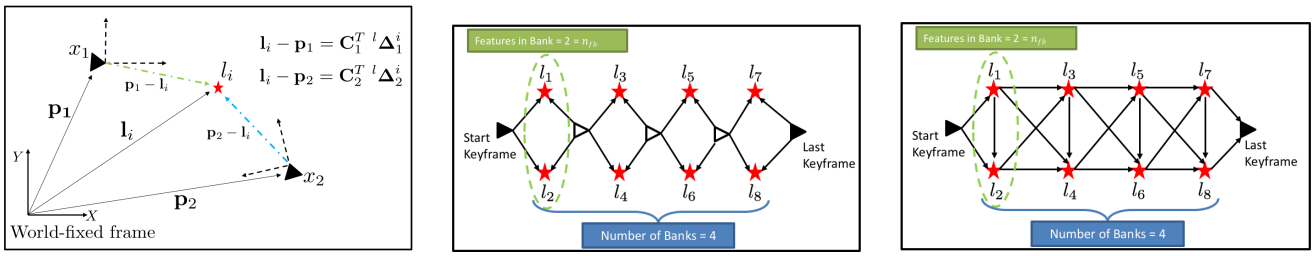

(a) A robot sees landmark l_i from two poses x_1, x_2 and estimates the relative positions ${}^l\mathbf{\Delta}_1^i$, ${}^l\mathbf{\Delta}_2^i$ of l_i in its local frames.

(b) R2F: Robot makes robot to feature relative position measurements.

(c) F2F: Robot makes relative feature to feature displacement measurements.

Fig. 1: Hypothetical scenarios depicting robot operation; (a) robot transforms local measurements to the global frame using orientation sensing; In (b) and (c) robot observes four banks of features prior to final pose with two features in each bank and uses approach R2F and F2F in (b) and (c) respectively.

studies to a 2D planar scenario which is explained by the nature of typical applications related to long-term navigation. However the problem formulation and method are easily generalizable to 3D applications. The effect of orientation is studied through two new formulations for feature-based SLAM. Further, we use the terms "error" and "error growth rate" in the scope of this work for the determinant of the position error covariance and its growth rate. Data associations to landmarks are assumed given and map is considered static. We leave the data association, dynamic map and obstacle avoidance problems to future extensions of this work.

IV. Methodology

In this section we develop two approaches for long-term localization that differ in the way measurements are processed:

1) **Robot to Feature Relative Position Measurement Model (R2F):** An approach designed for systems where a robot moves continuously and relies on odometery, orientation sensing and exteroceptive sensing like Lidar, cameras etc. This method converts local relative position measurements of features w.r.t robot at each pose to global frame measurements. These are then used to solve a linearized least squares estimation problem in robot and feature positions. Figure 1(b) depicts this approach.
2) **Feature to Feature Relative Measurement Model (F2F):** An approach designed for systems where odometery may not provide reliable information but time budgets may be higher. In this approach, independent measurements are made for relative displacements between features which are then chained together to estimate the map and robot position. Figure 1(c) depicts this approach.

A. R2F

The key steps of this approach are as follows:

1) Range bearing measurements to features are transformed to relative position estimates of features w.r.t robot at each pose (see Fig. 1(a)).
2) At keyframe poses, a linearized estimation problem is solved for the robot pose and features using the recorded data.
3) Once the estimation problem is solved, only correlations between keyframe poses and features observed at keyframe poses are maintained, intermediate feature and pose estimates are dropped.
4) An upper threshold is set on the number of keyframes to keep in the map after which the oldest keyframe is deleted (excluding first pose).

We now proceed to explain this approach in detail. Using the inverse measurement model g (Section III), we have the position of landmark l_i in robot's local frame as ${}^l\mathbf{\Delta}_k^i = {}^l\mathbf{g}(\mathbf{z}_k^i)$, extending this, the vector of local robot to feature relative position measurements is ${}^l\hat{\mathbf{\Delta}}_k = {}^l\mathbf{g}(\mathbf{z}_k)$. Thus ${}^l\hat{\mathbf{\Delta}}_k \sim \mathcal{N}({}^l\mathbf{\Delta}_k, {}^l\mathbf{R}_{\mathbf{\Delta}_k} = \bar{\nabla}{}^l\mathbf{g}|_{\mathbf{z}_k}\mathbf{R}_{\mathbf{z}_k}\bar{\nabla}{}^l\mathbf{g}^T|_{\mathbf{z}_k})$, where $\bar{\nabla}{}^l\mathbf{g}|_{\mathbf{z}_k}$ is the Jacobian of function ${}^l\mathbf{g}(\mathbf{z}_k)$. At t_0, we have keyframe ${}^{\kappa}x_0$, the robot starts moving and collecting odometery, orientation and exteroceptive measurements at each timestep. At some future timestep t_k, we have keyframe ${}^{\kappa}x_k$. Abusing notation slightly, let ${}^l\hat{\mathbf{\Delta}}_{0:k} \sim \mathcal{N}({}^l\mathbf{\Delta}_{0:k}, {}^l\mathbf{R}_{\mathbf{\Delta}_{0:k}})$ be the vector of all local relative position measurements (including robot to feature and translational odometery) recorded at poses $x_{0:k}$. At each t_k we have a noisy unbiased orientation measurement which gives us the vector $\hat{\boldsymbol{\theta}}_{0:k} \sim \mathcal{N}(\boldsymbol{\theta}_{0:k}, \mathbf{R}_{\boldsymbol{\theta}_{0:k}})$. Dropping the time subscript for readability, local relative measurements ${}^l\hat{\mathbf{\Delta}}$ can be transformed to the world frame as

$$ {}^w\hat{\mathbf{\Delta}} = \mathbf{C}^T(\hat{\boldsymbol{\theta}})\ {}^l\hat{\mathbf{\Delta}}, \tag{2} $$

where $\hat{\mathbf{C}} = \mathbf{C}(\hat{\boldsymbol{\theta}})$ is the corresponding composition of DCM matrices. From Eq. 2 it is clear that transformed global measurements at each pose $\mathbf{x}_k$ are correlated to heading measurement $\hat{\boldsymbol{\theta}}_k$. Heading error covariances must be propagated appropriately in the feature and robot position estimation. We setup a new measurement model $\boldsymbol{\beta} = \mathbf{h}_{\beta}({}^l\mathbf{\Delta}, \boldsymbol{\theta}) + \mathbf{v}_{\boldsymbol{\beta}}$ by stacking the transformed odometery between poses, robot to feature displacement and heading measurements. This gives us the following problem

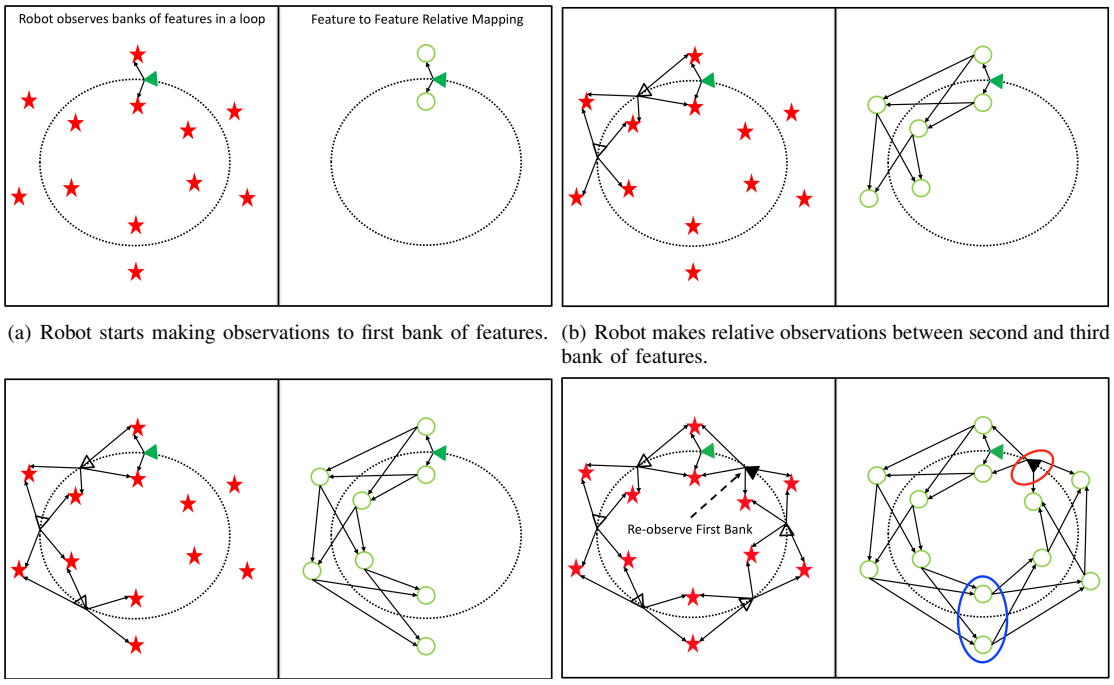

(a) Robot starts making observations to first bank of features.

(b) Robot makes relative observations between second and third bank of features.

(c) Robot is moving towards its start location.

(d) Robot re-observes the first bank of features.

Fig. 2: A simple graphical depiction of loop closure, the left half of each image shows the robot making range bearing measurements and the right half shows feature to feature mapping. In Fig. 2(d) we are interested in the estimation error of the farthest feature bank (encircled by blue ellipse) and the last pose (encircled by red ellipse).

$$\boldsymbol{\beta} = \begin{bmatrix} \hat{\mathbf{C}}^T \, {}^l\hat{\boldsymbol{\Delta}} \\ \hat{\boldsymbol{\theta}} \end{bmatrix} = \underbrace{\left[\begin{array}{c|c} \mathbf{A}' & \mathbf{0} \\ \hline \mathbf{0} & \mathbf{I} \end{array}\right]}_{\mathbf{A}} \left[\begin{array}{c} \mathbf{p} \\ \hline \mathbf{l} \\ \hline \boldsymbol{\theta} \end{array}\right] + \mathbf{v}_{\boldsymbol{\beta}}, \tag{3}$$

where $[\mathbf{p}^T, \mathbf{l}^T, \boldsymbol{\theta}^T]^T$ is the vector of robot poses, landmarks and heading, $\mathbf{A}'$ is a matrix with each row containing elements of the set $\{-1, 0, +1\}$, $\mathbf{v}_{\boldsymbol{\beta}} \sim \mathcal{N}(\mathbf{0}, \mathbf{R}_{\boldsymbol{\beta}})$ is the measurement noise vector with covariance

$$\mathbf{R}_{\boldsymbol{\beta}} = \bar{\nabla}\mathbf{h}_\beta \begin{bmatrix} {}^l\mathbf{R}_{\boldsymbol{\Delta}} & \mathbf{0} \\ \mathbf{0} & \boldsymbol{\Sigma}_{\boldsymbol{\theta}} \end{bmatrix} \bar{\nabla}^T\mathbf{h}_\beta, \tag{4}$$

where $\bar{\nabla}\mathbf{h}_\beta$ is the Jacobian of measurement function $\mathbf{h}_\beta$ given by

$$\bar{\nabla}\mathbf{h}_\beta = \begin{bmatrix} \mathbf{C}^T & \mathbf{M} \, {}^l\hat{\boldsymbol{\Delta}} \\ \mathbf{0} & \mathbf{I} \end{bmatrix}, \; \mathbf{M} = \frac{\partial \hat{\mathbf{C}}^T}{\partial \boldsymbol{\theta}}|_{\boldsymbol{\theta}=\hat{\boldsymbol{\theta}}}. \tag{5}$$

The solution to the problem in Eq. 3 is given by

$$\begin{bmatrix} \mathbf{p}^* \\ \mathbf{l}^* \\ \boldsymbol{\theta}^* \end{bmatrix} = (\mathbf{A}^T\mathbf{R}_{\boldsymbol{\beta}}^{-1}\mathbf{A})^{-1}\mathbf{A}^T\mathbf{R}_{\boldsymbol{\beta}}^{-1}\boldsymbol{\beta}. \tag{6}$$

From Eq. 6 we are interested in $\mathbf{p}^*$ and $\mathbf{l}^*$.

1) Analysis: We analyze localization accuracy for approach R2F as a robot explores an unknown map and the effect of loop closure. We assume that relative measurements from robot to features in the global frame are independent; for orientations sensors such as star trackers which are highly precise such an assumption holds quite well. For clarity of presentation and ease of understanding error covariance of every global relative measurement is assumed to be $\mathbf{R}_a$. In this analysis, the first and last pose of the robot are considered as keyframes with first pose known.

Exploration: In an exploration task, a robot moves into unknown areas and makes measurements to a bank of features at each timestep as shown in Fig. 1(b). A bank is simply the set of features observed at a particular pose. Figure 3(a) shows that the error growth is linear as robot moves further away from its initial pose. An interesting point arises in Fig. 3(b), the rate of error growth drops as $\propto 1/n_{fb}$ where n_{fb} is the number of features in each bank. Thus it implies that for long-term autonomy, it benefits us to make high-quality observations to a large number of features but we may not always need hundreds or thousands of features. Rather one may predict localization error for a given task and decide how many features to observe. This can help in constraining computational complexity and memory resources.

Loop Closure: Loop closure is usually considered a necessity in SLAM to limit error growth. We consider the effect of loop

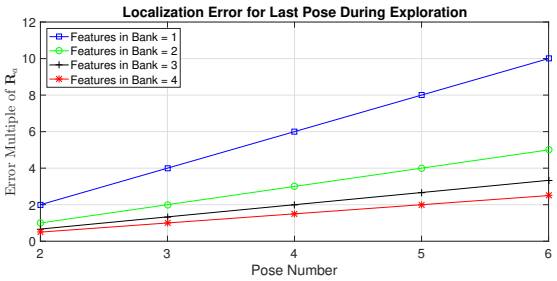

(a) The error growth in estimate of final pose as a function of how far the robot moves.

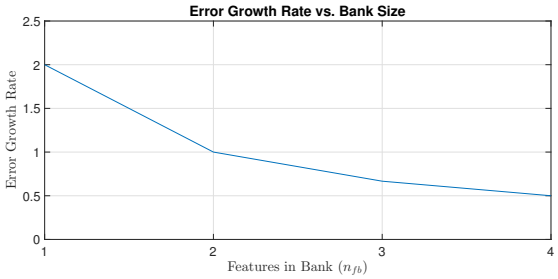

(b) The position estimation error growth rate drops $\propto 1/n_{fb}$ as the number of landmarks in each bank n_{fb} increases.

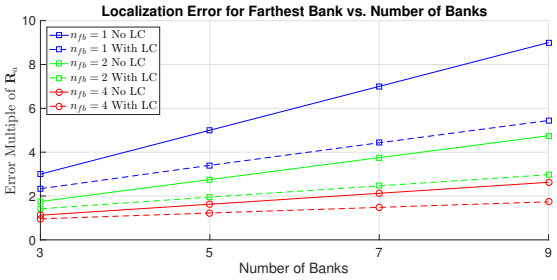

(c) Localization error in the feature bank farthest from start before (solid lines) and after (dashed lines) loop closure.

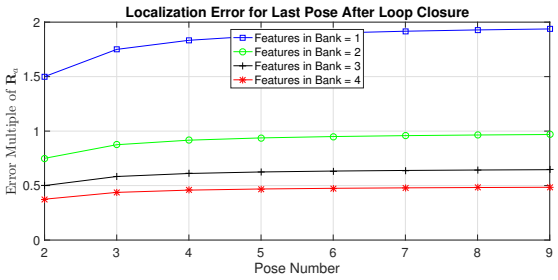

(d) Localization error in the last pose after loop closure as the trajectory length (number of banks mapped) increases.

Fig. 3: **R2F:** Analysis of the pose and map estimation error (determinant of position error covariance) as the robot explores unknown regions and the effect of loop closure when robot re-observes features mapped at first pose.

closure on the bank of features farthest from the start location in a loop and on the last pose (see Fig. 2):

1) For the error in farthest bank (encircled by a blue ellipse in Fig. 2(d)), Fig. 3(c) shows that the effect of loop closure diminishes as the bank size increases (slope of solid vs. dashed lines). Note that the ratio of error growth rate after and before loop closure is 0.5185, i.e., loop closure approximately halves the error growth in the farthest bank.
2) Figure 3(d) shows that error in last pose after loop closure converges to a fixed value as the trajectory length increases.

The first observation noted above can be understood intuitively. Looking at Fig. 2(d), there are two "pathways" that link the farthest bank of features to the first bank. Prior to loop closure there is only one path for the relative measurements to constrain feature estimates to the first bank, however, after loop closure there is a second pathway from the opposite direction. If we were to take two observations ($\mathbf{R}_a$ is halved) for each feature, we would effectively end up with the same estimation error at the farthest bank were the robot not to close the loop. The second observation tells us that the estimation error in the last bank of features is dominated by the relative measurement to the first bank, i.e., as the trajectory length grows, the effect of the longer "pathway" from start has almost no effect on estimation accuracy.

B. F2F

The key steps in approach F2F are as follows:

1) As the robot moves, range bearing measurements to features are transformed into relative displacement estimates between features.
2) Robot to feature relative position measurements are acquired at keyframes. Then a linearized estimation problem is solved for keyframe poses and map features using the recorded data.
3) Once the estimation problem is solved, only correlations between keyframe poses and features observed at keyframes are maintained, intermediate feature estimates are dropped.
4) An upper threshold is set on the number of keyframes to keep in the map after which the oldest keyframe is deleted (excluding first pose).

We now proceed to explain this approach in detail. At time t_k we have the measurement of displacement vector from l_i to l_j in the robot frame as

$$ {}^{l}\mathbf{d}_k^{ij} = {}^{l}\boldsymbol{\Delta}_k^{j} - {}^{l}\boldsymbol{\Delta}_k^{i} = {}^{l}\mathbf{g}_d(\mathbf{z}_k^j, \mathbf{z}_k^i). \tag{7} $$

The above equation shows that ${}^{l}\mathbf{d}_k^{ij}$ is independent of robot position $\mathbf{p}_k$ and orientation $\boldsymbol{\theta}_k$. The vector of local relative measurements is ${}^{l}\hat{\mathbf{d}}_k = {}^{l}\mathbf{g}_d(\mathbf{z}_k)$. Note that though range bearing measurements to each feature are independent, the set of relative feature measurements may be *correlated* in a naive implementation due to the correlations between relative measurements using the same range-bearing observation. This is where a key difference from existing methods arises; our method takes independent relative measurements by capturing sufficient range bearing observations to features.

Let ${}^{l}\hat{\mathbf{d}}_k \sim \mathcal{N}({}^{l}\mathbf{d}_k, {}^{l}\mathbf{R}_{\mathbf{d}_k} = \bar{\nabla}{}^{l}\mathbf{g}_d|_{\mathbf{z}_k}\mathbf{R}_{\mathbf{z}_k}\bar{\nabla}{}^{l}\mathbf{g}_d^T|_{\mathbf{z}_k})$ be the vector of independent relative feature measurements at time t_k with error covariance ${}^{l}\mathbf{R}_{\mathbf{d}_k}$, where $\bar{\nabla}{}^{l}\mathbf{g}_d|_{\mathbf{z}_k}$ is the Jacobian of the local relative measurement function ${}^{l}\mathbf{g}_d(\mathbf{z}_k)$. The robot collects orientation and exteroceptive measurements at each timestep. At some future timestep t_k, we have keyframe ${}^{\kappa}x_k$. Dropping the time subscript for legibility. Let ${}^{l}\hat{\mathbf{d}} \sim \mathcal{N}({}^{l}\mathbf{d}, {}^{l}\mathbf{R}_{\mathbf{d}})$ be the vector of local relative feature to feature measurements captured from time t_1 to t_k. At keyframes ${}^{\kappa}x_0$ and ${}^{\kappa}x_k$ we have robot to feature relative measurements which give us ${}^{l}\hat{\mathbf{\Delta}} \sim \mathcal{N}({}^{l}\mathbf{\Delta}, {}^{l}\mathbf{R}_{\mathbf{\Delta}})$. At each pose we have a noisy unbiased heading measurement which provides the vector of orientation estimates $\hat{\boldsymbol{\theta}} \sim \mathcal{N}(\boldsymbol{\theta}, \mathbf{R}_{\boldsymbol{\theta}})$. The vectors of local relative measurements ${}^{l}\hat{\mathbf{\Delta}}, {}^{l}\hat{\mathbf{d}}$ can be transformed to the world frame as

$$\begin{bmatrix} {}^{w}\hat{\mathbf{d}} \\ {}^{w}\hat{\mathbf{\Delta}} \end{bmatrix} = \hat{\mathbf{C}}^T \begin{bmatrix} {}^{l}\hat{\mathbf{d}} \\ {}^{l}\hat{\mathbf{\Delta}} \end{bmatrix}. \tag{8}$$

Heading error covariances must be propagated appropriately in the feature and robot position estimation. Thus we setup a new measurement model $\boldsymbol{\gamma} = \mathbf{h}_\gamma({}^{l}\mathbf{\Delta}, {}^{l}\mathbf{d}, \boldsymbol{\theta}) + \mathbf{v}_{\boldsymbol{\gamma}}$ by stacking the transformed relative position and heading measurements. This gives us the following problem

$$\boldsymbol{\gamma} = \begin{bmatrix} \hat{\mathbf{C}}^T\,{}^{l}\hat{\mathbf{d}} \\ \hat{\mathbf{C}}^T\,{}^{l}\hat{\mathbf{\Delta}} \\ \hat{\boldsymbol{\theta}} \end{bmatrix} = \underbrace{\left[\begin{array}{c|c} \mathbf{A}' & \mathbf{0} \\ \hline \mathbf{0} & \mathbf{I} \end{array}\right]}_{\mathbf{A}} \begin{bmatrix} \mathbf{l} \\ \mathbf{p} \\ \hline \boldsymbol{\theta} \end{bmatrix} + \mathbf{v}_{\boldsymbol{\gamma}}, \tag{9}$$

where $[\mathbf{l}^T, \mathbf{p}^T, \boldsymbol{\theta}^T]^T$ is the vector of landmark positions, robot poses and heading, $\mathbf{A}'$ is a matrix with each row containing elements of the set $\{-1, 0, +1\}$, $\mathbf{v}_\gamma \sim \mathcal{N}(\mathbf{0}, \mathbf{R}_{\boldsymbol{\gamma}})$ is the measurement noise vector where

$$\mathbf{R}_{\boldsymbol{\gamma}} = \bar{\nabla}\mathbf{h}_\gamma \begin{bmatrix} {}^{l}\mathbf{R}_{\mathbf{d}} & \mathbf{0} & \mathbf{0} \\ \mathbf{0} & {}^{l}\mathbf{R}_{\mathbf{\Delta}} & \mathbf{0} \\ \mathbf{0} & \mathbf{0} & \mathbf{\Sigma}_{\boldsymbol{\theta}} \end{bmatrix} \bar{\nabla}^T\mathbf{h}_\gamma. \tag{10}$$

$\bar{\nabla}\mathbf{h}_\gamma$ is the Jacobian of measurement function $\mathbf{h}_\gamma$ given by

$$\bar{\nabla}\mathbf{h}_\gamma = \begin{bmatrix} \mathbf{0} & \mathbf{C}^T & \mathbf{M}\,{}^{l}\hat{\mathbf{d}} \\ \mathbf{C}^T & \mathbf{0} & \mathbf{M}\,{}^{l}\hat{\mathbf{\Delta}} \\ \mathbf{0} & \mathbf{0} & \mathbf{I} \end{bmatrix}, \text{where } \mathbf{M} = \frac{\partial \hat{\mathbf{C}}^T}{\partial \boldsymbol{\theta}}|_{\boldsymbol{\theta}=\hat{\boldsymbol{\theta}}}. \tag{11}$$

The solution to the problem in Eq. 9 is given by

$$\begin{bmatrix} \mathbf{l}^* \\ \mathbf{p}^* \\ \boldsymbol{\theta}^* \end{bmatrix} = (\mathbf{A}^T\mathbf{R}_{\boldsymbol{\gamma}}^{-1}\mathbf{A})^{-1}\mathbf{A}^T\mathbf{R}_{\boldsymbol{\gamma}}^{-1}\boldsymbol{\gamma}. \tag{12}$$

1) Analysis: We proceed to analyze how the localization error grows as a robot explores an unknown map and the affect of loop closure with approach F2F. By virtue of the reasoning provided in Section IV-A1, it is assumed that the global frame relative feature measurements are independent and error covariance of every global relative measurement is $\mathbf{R}_a$. Again, the first and last pose of the robot are considered as keyframes with the first pose known.

Exploration: We analytically solve the estimation problem of Eq. 9 and compute error covariance for multiple cases by varying bank size n_{fb} and the number of banks that the robot maps. Figure 4 shows our results, the plots highlight two key points:

1) Figure 4(a) shows that localization error grows linearly as the robot moves away from the start location.
2) The error growth rate shown in Fig. 4(b) is inversely proportional to the square of the size of each feature bank, i.e., $\propto \frac{1}{n_{fb}^2}$ where n_{fb} is the number features in one bank. Thus error growth with F2F is $\frac{1}{n_{fb}}$-th of the error growth with R2F.

Loop Closure: Figure 2 depicts loop closure when a robot makes relative feature measurements while moving in a circular trajectory. Our goal is to understand the effect of loop closure on mapping accuracy, particularly error in estimation of farthest feature bank from start and last keyframe at which robot re-observes landmarks seen at its starting location (see Fig. 2(d)). We solve Eq. 9 with loop closure. The results of this analysis are plotted in Figs. 4(c) and 4(d); the key points to be noted are:

1) The ratio of error growth rate with loop closure to error growth rate without loop closure is a constant value of 0.5181 for all values of n_{fb} computed as the ratio of slopes of curves plotted in Fig. 4(c) before and after loop closure.
2) Figure 4(d) shows that error in last pose after loop closure converges to a fixed value as the trajectory length (number of banks) increases.

Thus the behavior of loop closure with method F2F is similar to that with R2F, i.e., loop closure halves the estimation error of farthest feature bank and error in last pose estimate is dominated by measurement to the first bank of features.

V. Results

Simulation results are presented for waypoint following in a 2D environment. These simulations study the case of a long term exploration task where a robot may not visit prior locations. Robot kinematics are modeled as a steered bicycle [11]. The robot moves at a speed of 10 m/s and simulation time step is 0.05 s. Keyframes are recorded every 100 time steps or 5 s, and a maximum of 4 keyframes are kept in memory. The robot is equipped with three sensors; star tracker with noise standard deviation $\sigma_\theta = 0.005^\circ$ (18 arcseconds); range bearing sensor with a 360° field-of-view, range of 20 m and noise standard deviation of $\sigma_r = 0.1$ m in range and $\sigma_\phi = 1.0^\circ$ in bearing; wheel odometery noise is scaled according to factor $\alpha = \{1, 2, 3, 4\}$ with $\alpha = 4$ corresponding to noise standard deviation $\sigma_{\delta x, \delta y} = 0.1$ m in translation and $\sigma_{\delta\theta} = 1.2^\circ$ in rotation. Two different scenarios are presented:

1) **Scenario A:** A 2D world (5 km$\times 5$ km) with a trajectory of length 25.9 km as depicted in Fig. 5(a).

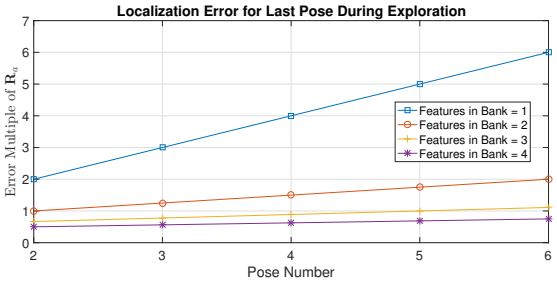

(a) The error growth in estimate of the last pose as a function of how far the robot moves. The growth is linear as robot moves away from its start.

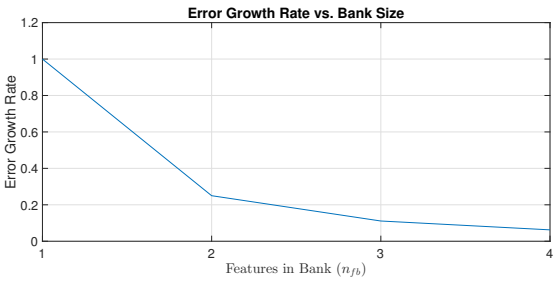

(b) The error growth rate drops sharply $\propto 1/n_{fb}^2$ as the number of landmarks in each bank n_{fb} increases.

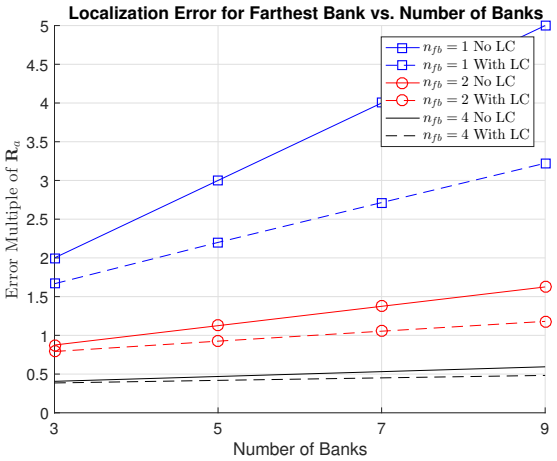

(c) Localization error in the bank farthest from start before (solid lines) and after (dashed lines) loop closure.

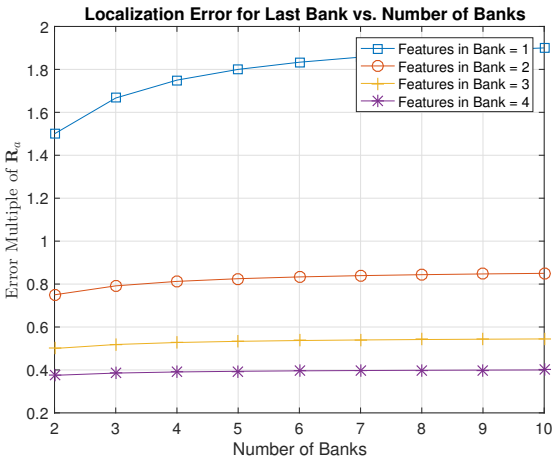

(d) Localization error in the last bank after loop closure as the trajectory length (number of banks mapped) increases.

Fig. 4: **F2F:** Analysis of the feature mapping and localization error (determinant of position error covariance) as the robot moves and the effect of loop closure.

2) **Scenario B:** A 2D world (10 km $\times$ 10 km) with a trajectory of length 107.9 km as depicted in Fig. 5(b).

For each scenario, multiple versions of the environments were generated by varying n_{fb}, i.e., the minimum number of features visible at each pose and then randomly sampling feature locations. Simulations results for a robot equipped only with wheel odometery and orientation sensing are plotted in Fig. 6 for both scenarios. In simulations for method R2F, only the highest odometery noise level, i.e., $\alpha = 4$ is considered, further recall that method F2F does not require odometery. Finally, results for approaches R2F and F2F are plotted in Figures 7 and 8 for scenarios A and B respectively. In total, 1200 simulations were conducted.

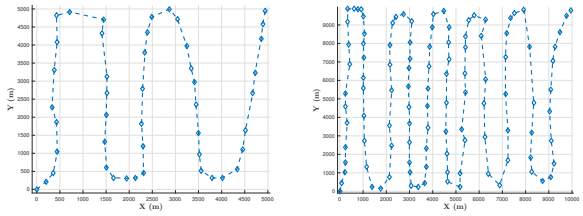

(a) Scenario A with 25.9 km trajectory.

(b) Scenario B with 107.9 km trajectory.

Fig. 5: The robot is tasked to follow the waypoints (depicted by diamonds) sequentially. Note that the trajectory terminates far from the start location and there are no loop closures in the trajectory by design.

A. Discussion

For a robot equipped only with odometery and orientation sensing (Fig. 6) with $\alpha = 4$, in scenario A error is 27.63 m and in scenario B error is 56 m. Worst case error ($n_{fb} = 4$) in scenario A for method R2F (1.12 m) and F2F (0.55 m) and for scenario B with method R2F (2.36 m) and F2F (1.14 m) are on average $1-2$ orders of magnitude lower. Note that odometery noise at 1σ corresponds to 20% error in relative position estimate for motion in a single time step which is relatively high, however in practical applications wheel slip may go as high as 125% [26] (steep gradients, loose gravel or soil may cause wheel spin in-place). While using odometery with orientation performs reasonably, it may not meet requirements for certain missions, be reliable or robust in practical applications and may not scale well with longer trajectories. Using measurements to features on the other hand betters performance while making our method robust and

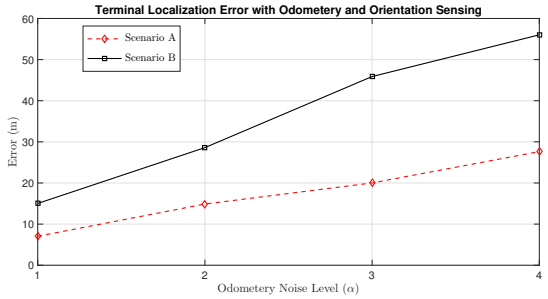

Fig. 6: The average terminal localization error in Scenarios A and B when robot uses an absolute orientation sensor coupled with odometery.

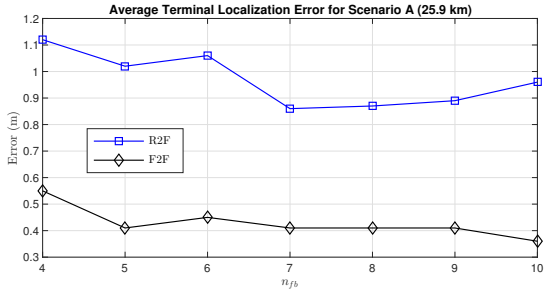

(a) Average terminal localization error for proposed approaches.

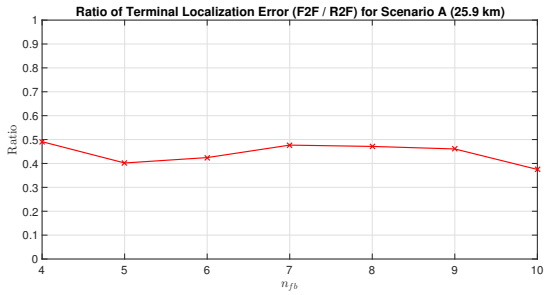

(b) Ratio of error with approach F2F to approach R2F.

Fig. 7: Scenario A: (a) Average terminal localization error; and (b) ratio of localization error with F2F to error with R2F as the minimum number of features (n_{fb}) visible at each pose is varied. R2F results are depicted in blue with square markers and F2F in black with diamond markers.

allows control over the error growth rate.

Figure 7(a) shows the reduction in localization error at the final waypoint in scenario A (25.9 km), for approach R2F and F2F. R2F results in a 23.2% error reduction from 1.12 m at $n_{fb} = 4$ to 0.86 m at $n_{fb} = 7$. There is a minor 0.1 m increase in error from $n_{fb} = 7$ to $n_{fb} = 10$ which can be attributed to the random placement of landmarks; recall that in the physical world error in relative position measurements to features is governed by the range and bearing to a feature, i.e., a far feature's relative position estimate w.r.t robot is more sensitive to error in bearing measurement than a closer feature. With F2F error reduces by 34.5% from 0.55 m at $n_{fb} = 4$ to 0.36 m at $n_{fb} = 10$. Figure 7(b) shows that

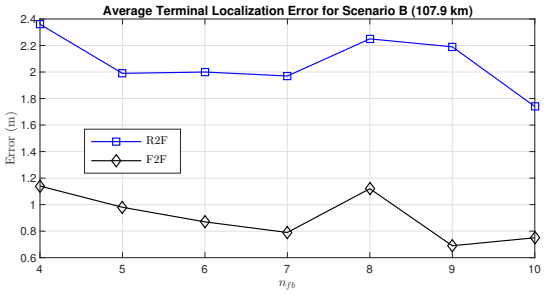

(a) Average terminal localization error for the two proposed approaches.

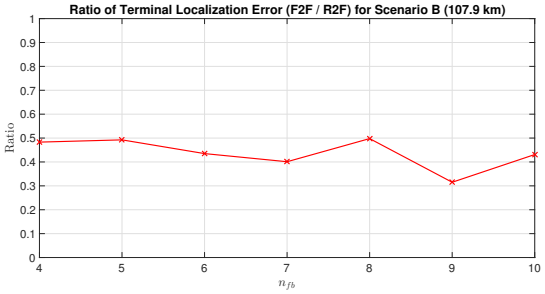

(b) Ratio of error with approach F2F to approach R2F.

Fig. 8: Scenario B: (a) Average terminal localization error; and (b) ratio of localization error with F2F to error with R2F as the minimum number of features (n_{fb}) visible at each pose is varied.

F2F results in $40-50\%$ error relative to R2F, recall that F2F does not incorporate odometery. This supports findings of MER missions [26] wherein wheel slip on high-gradient slopes require the rover to rely on visual odometery to estimate motion. Figure 8 depicts localization error at the final waypoint in scenario B (107.9 km), for approach R2F and F2F. R2F results in a 26.3% error reduction from 2.36 m at $n_{fb} = 4$ to 1.74 m at $n_{fb} = 10$. F2F results in a 29.6% reduction in error from 0.98 m at $n_{fb} = 4$ to 0.69 m at $n_{fb} = 9$. Figure 8(b) shows that F2F results in $40-50\%$ error relative to R2F similar to scenario A.

Compared to existing methods that rely on absolute orientation sensing, our approach results in order(s) of magnitude better performance. The method of [31] fuses inertial sensing with star tracking for autonomous navigation and demonstrated a localization error of ≈ 2 m for a ≈ 3.8 km trajectory[1]. In the lunar positioning method of [27], for the case of tilt estimation error in both roll and pitch axes of $0.05°$, star tracker boresight accuracy of $0.0014°$, and boresight roll of $0.01°$, the resulting error is 1.2 km. The approach of [28] using a sun sensor fused with inertial data and wheel odometery for navigation resulted in a 6% cross-track position error for 1 km of driving.

VI. Conclusions and Future Work

Two approaches for feature-based localization and mapping were developed for the case when global orientation sensing

[1]Numerical values ascertained from graphical plots in [31] to the best of our understanding.

is available. In method R2F, localization error growth rate is $\propto 1/n_{fb}$, and for method F2F error growth rate is $\propto 1/n_{fb}^2$, where n_{fb} is the minimum number of features visible to a robot at each time. Analysis for both methods shows that; (i) given unbiased heading measurements, localization error growth is linear as robot moves away from its start location; and (ii) loop closure results in $\approx 50\%$ reduction in localization error of features farthest from loop start location. Analysis also indicates that estimation accuracy may be enhanced by taking prolonged measurements which is more suitable for a point-to-point navigation task, thus avoiding loop closure when absolute heading is available. Simulations show that using the proposed approaches order(s) of magnitude better performance is achievable, i.e., with as low as 9 features being tracked at any time, a robot can achieve a position accuracy of 0.69 m for > 100 km of driving. Future work would investigate planning to incorporate obstacles, unknown data associations and terminal localization error constraints. A secondary goal of this work is to nudge SLAM research to explore absolute orientation sensing, particularly the development of promising sensors such as daylight star trackers and MEMS-based gyrocompasses along with their application to autonomous navigation for mobile robots.

REFERENCES

[1] S. Thrun, W. Burgard, and D. Fox, *Probabilistic Robotics*. MIT Press, 2005.

[2] E. Jones and S. Soatto, "Visual-inertial navigation, mapping and localization: A scalable real-time causal approach," *International Journal of Robotics Research*, January 2011.

[3] M. Li and A. I. Mourikis, "High-precision, consistent ekf-based visualinertial odometry," *The International Journal of Robotics Research*, vol. 32, no. 6, pp. 690–711, 2013.

[4] Ln-120g stellar-inertial-gps navigation. [Online]. Available: http://www.northropgrumman.com

[5] F. Pappalardi, S. J. Dunham, M. E. LeBlang, T. E. Jones, J. Bangert, and G. Kaplan, "Alternatives to gps," in *OCEANS, 2001. MTS/IEEE Conference and Exhibition*, vol. 3, 2001, pp. 1452–1459 vol.3.

[6] R. Smith, M. Self, and P. Cheeseman, "A stochastic map for uncertain spatial relationships," in *Proceedings of the 4th International Symposium on Robotics Research*. Cambridge, MA, USA: MIT Press, 1988, pp. 467–474. [Online]. Available: http://dl.acm.org/citation.cfm?id=57425.57472

[7] A. Mourikis and S. Roumeliotis, "Analytical characterization of the accuracy of slam without absolute orientation measurements," in *Proceedings of Robotics: Science and Systems*, Philadelphia, USA, August 2006.

[8] G. P. Huang, A. I. Mourikis, and S. I. Roumeliotis, "Observability-based rules for designing consistent ekf slam estimators," *The International Journal of Robotics Research*, vol. 29, no. 5, pp. 502–528, 2009.

[9] J. Castellanos, J. Neira, and J. Tardos, "Limits to the consistency of ekf-based slam," in *In IFAC Symposium on Intelligent Autonomous Vehicles*, 2004.

[10] S. Huang and G. Dissanayake, "Convergence and consistency analysis for extended kalman filter based slam," *IEEE Transactions on Robotics*, vol. 23, no. 5, pp. 1036–1049, Oct 2007.

[11] T. Bailey, J. Nieto, J. Guivant, M. Stevens, and E. Nebot, "Consistency of the ekf-slam algorithm," in *Intelligent Robots and Systems, 2006 IEEE/RSJ International Conference on*, Oct 2006, pp. 3562–3568.

[12] S. J. Julier and J. K. Uhlmann, "A counter example to the theory of simultaneous localization and map building," in *Robotics and Automation, 2001. Proceedings 2001 ICRA. IEEE International Conference on*, vol. 4, 2001, pp. 4238–4243 vol.4.

[13] F. Lu and E. Milios, "Globally consistent range scan alignment for environment mapping," *Auton. Robots*, vol. 4, no. 4, pp. 333–349, Oct. 1997.

[14] S. Thrun and M. Montemerlo, "The graph slam algorithm with applications to large-scale mapping of urban structures," *The International Journal of Robotics Research*, vol. 25, no. 5-6, pp. 403–429, 2006. [Online]. Available: http://ijr.sagepub.com/content/25/5-6/403.abstract

[15] F. Dellaert and M. Kaess, "Square root sam: Simultaneous localization and mapping via square root information smoothing," *The International Journal of Robotics Research*, vol. 25, no. 12, pp. 1181–1203, 2006.

[16] K. Konolige, G. Grisetti, R. Kmmerle, W. Burgard, B. Limketkai, and R. Vincent, "Efficient sparse pose adjustment for 2d mapping," in *Intelligent Robots and Systems (IROS), 2010 IEEE/RSJ International Conference on*, Oct 2010, pp. 22–29.

[17] J. Folkesson and H. Christensen, "Graphical slam - a self-correcting map," in *Robotics and Automation, 2004. Proceedings. ICRA '04. 2004 IEEE International Conference on*, vol. 1, April 2004, pp. 383–390 Vol.1.

[18] L. Carlone, R. Aragues, J. A. Castellanos, and B. Bona, "A fast and accurate approximation for planar pose graph optimization," *The International Journal of Robotics Research*, vol. 33, no. 7, pp. 965–987, 2014.

[19] L. Carlone and A. Censi, "From angular manifolds to the integer lattice: Guaranteed orientation estimation with application to pose graph optimization," *IEEE Transactions on Robotics*, vol. 30, no. 2, pp. 475–492, April 2014.

[20] K. Khosoussi, S. Huang, and G. Dissanayake, "Exploiting the separable structure of slam," in *Proceedings of Robotics: Science and Systems*, Rome, Italy, July 2015.

[21] S. Agarwal, V. Shree, and S. Chakravorty, "Rfm-slam: Exploiting relative feature measurements to separate orientation and position estimation in slam," in *Proc. IEEE International Conference on Robotics and Automation (ICRA).*, May 29 - June 3 2017.

[22] L. Carlone, G. C. Calafiore, C. Tommolillo, and F. Dellaert, "Planar pose graph optimization: Duality, optimal solutions, and verification," *IEEE Transactions on*

Robotics, vol. 32, no. 3, pp. 545–565, June 2016.

[23] D. Rosen, L. Carlone, A. Bandeira, and J. Leonard, "A certifiably correct algorithm for synchronization over the special Euclidean group," in *Intl. Workshop on the Algorithmic Foundations of Robotics (WAFR)*, San Francisco, CA, Dec. 2016.

[24] Star tracker st400 and st200. [Online]. Available: https://www.berlin-space-tech.com/portfolio/star-tracker-st400-and-st200/

[25] D. Mortari, "A fast on-board autonomous attitude determination system based on a new star-id technique for a wide fov star tracker," in *Sixth Annual AIAA/AAS Space Flight Mechanics Meeting, Austin, TX*, February 1996.

[26] M. Maimone, Y. Cheng, and L. Matthies, "Two years of visual odometry on the mars exploration rovers," *Journal of Field Robotics*, vol. 24, no. 3, pp. 169–186, 2007. [Online]. Available: http://dx.doi.org/10.1002/rob.20184

[27] D. A. Sigel and D. Wettergreen, "Star tracker celestial localization system for a lunar rover," in *2007 IEEE/RSJ International Conference on Intelligent Robots and Systems*.

[28] R. Volpe, "Navigation results from desert field tests of the rocky 7 mars rover prototype," *The International Journal of Robotics Research*, vol. 18, no. 7, pp. 669–683, 1999. [Online]. Available: http://ijr.sagepub.com/content/18/7/669.abstract

[29] A. Trebi-Ollennu, T. Huntsberger, Y. Cheng, E. T. Baumgartner, B. Kennedy, and P. Schenker, "Design and analysis of a sun sensor for planetary rover absolute heading detection," *IEEE Transactions on Robotics and Automation*, vol. 17, no. 6, pp. 939–947, Dec 2001.

[30] P. Furgale, J. Enright, and T. Barfoot, "Sun sensor navigation for planetary rovers: Theory and field testing," *IEEE Transactions on Aerospace and Electronic Systems*, vol. 47, no. 3, pp. 1631–1647, July 2011.

[31] X. Guan, X. Wang, J. Fang, and S. Feng, "An innovative high accuracy autonomous navigation method for the mars rovers," *Acta Astronautica*, vol. 104, no. 1, pp. 266 – 275, 2014.

[32] I. P. Prikhodko, S. A. Zotov, A. A. Trusov, and A. M. Shkel, "What is mems gyrocompassing? comparative analysis of maytagging and carouseling," *Journal of Microelectromechanical Systems*, vol. 22, no. 6, pp. 1257–1266, December 2013.

[33] Stellar-inertial navigation system. [Online]. Available: http://www.northropgrumman.com